

J-Bio NMR 458

Side-chain conformation and dynamics in a solid peptide: CP-MAS NMR study of valine rotamers and methyl-group relaxation in fully ^{13}C -labelled antamanide

Suzana K. Straus, Tobias Breimi and Richard R. Ernst*

Laboratorium für Physikalische Chemie, ETH Zentrum, CH-8092 Zürich, Switzerland

Received 4 March 1997

Accepted 10 April 1997

Keywords: Solid-state NMR; Peptide dynamics; Side-chain conformation; Methyl-group relaxation; Homonuclear decoupling; Stereospecific assignment

Summary

The effect of the crystal lattice on the side-chain conformation and side-chain dynamics in peptides is investigated by solid-state NMR, using the cyclic decapeptide antamanide as an example. The study takes advantage of the ^{13}C assignment of the backbone and side chains based on the resolution-enhanced 2D spin-diffusion spectra by heteronuclear and homonuclear decoupling. The spectra even allow for a stereospecific assignment of the γ -carbons of the valine residue. It is found that the valine side chain coexists in two static rotamer conformations which have not been observed by X-ray crystallography. In addition, remarkable effects of the crystal packing on the methyl-group rotation frequency are found from ^{13}C relaxation measurements.

Introduction

Today X-ray crystallography is the most powerful and most successful technique for the determination of the solid-state structure of biomolecules and of supramolecular assemblies. At first glance, it seems unnecessary to contemplate further the possible usage of alternative techniques. However, X-ray crystallography also has its limitations. Firstly, it is dependent on the availability of single crystals of sufficient quality. Especially for membrane proteins, single crystals prove to be difficult to obtain, and solution studies are, for solubility reasons, not yet feasible. Moreover, even with high-quality single crystals available, it is impossible to properly assess intramolecular dynamics by X-ray crystallography. It is becoming more and more clear that biomolecular interactions and activity are significantly influenced by molecular flexibility and it is necessary to develop proper tools for the study of intramolecular dynamic phenomena.

These are the reasons for exploring the possibilities of NMR for the study of structural and dynamical features of biomolecules in the solid state. Biomolecular solid-state

NMR is already a very active field of science (Frey et al., 1985; Opella et al., 1987; Stewart et al., 1988; Griffiths et al., 1995; Lansbury et al., 1995; Lazo and Cross, 1995; Naito et al., 1995; Heller et al., 1996; Hirsh et al., 1996). Many studies use site-selectively isotope-labelled molecules to address specific structural or dynamical questions, thereby avoiding the need for a full assignment of all resonances (Griffiths et al., 1995; Lansbury et al., 1995; Heller et al., 1996; Hirsh et al., 1996). For more comprehensive NMR investigations, a full assignment of the resonances is indispensable. Because of the limited resolution of proton resonances in the solid state, it is necessary to base the sequential assignment of peptides and proteins on the connectivity of carbon and nitrogen nuclei in fully ^{13}C - and ^{15}N -labelled samples. The resulting additional spin-spin interactions among the heteronuclei further reduce the already limited spectral resolution in the solid state.

Fortunately, significant advances have recently been made in improving the spectral resolution of magic angle spinning (MAS) NMR spectra of fully ^{13}C - and ^{15}N -labelled biomolecules. First, heteronuclear proton decoupling

*To whom correspondence should be addressed.

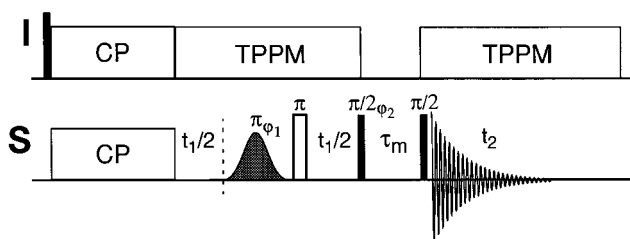


Fig. 1. Pulse sequence to correlate the ^{13}C chemical shifts by proton-driven spin diffusion, with homonuclear decoupling in ω_1 . All pulses except the shaped one are high-power ($\omega_1/2\pi = 71.4$ kHz; $\omega_s/2\pi = 65.8$ kHz). The low-power Gaussian pulse is described in the text. Heteronuclear proton decoupling is achieved using TPPM. The minimal phase cycle, resulting in artefact-free spectra with subtraction of all out-of-band resonances, is $\phi_1 = x, y$, receiver phase = $x, -x$. Quadrature detection in t_1 is achieved by TPPI, incrementing ϕ_2 .

by the TPPM sequence (Bennett et al., 1995) removes very efficiently the heteronuclear broadening, and, secondly, it is possible to suppress also the ^{13}C - ^{13}C interactions by homonuclear decoupling (Straus et al., 1996). These innovations open up possibilities for a full resonance assignment.

The present investigation of a motional process in a prototype peptide takes advantage of the attainability of the full resonance assignment in the solid state and serves as an example for demonstrating the capabilities of modern solid-state NMR. In addition, it puts into evidence the influence of the solid-state environment on the side-chain conformation and the side-chain mobility in peptides.

For this investigation, we have selected antamanide, a cyclic decapeptide (-Val¹-Pro²-Pro³-Ala⁴-Phe⁵-Phe⁶-Pro⁷-Pro⁸-Phe⁹-Phe¹⁰-) that has been studied extensively before by solution NMR (Burgermeister et al., 1974; Müller, 1986; Kessler et al., 1987, 1988, 1989a, b; Mádi et al., 1990; Brüsweiler et al., 1991, 1992; Blackledge et al., 1993; Schmidt et al., 1993; Bremi et al., 1994; Ernst et al., 1996; Schmidt, 1997) and by X-ray crystallography (Karle et al., 1979). The question to be addressed concerns the environmental effects on the side-chain conformation of Val¹ and on the methyl-group rotation. For availability reasons, the assignment had to be based on a ^{13}C only labelled sample. It includes the stereospecific assignment of the Val¹ methyl groups.

Experimental

^{13}C -labelled (99%) antamanide was synthesized by Prof. S. Aimoto, Institute of Protein Research, Osaka University, Japan, based on labelled amino acids supplied by Prof. M. Kainosho, Department of Chemistry, Tokyo Metropolitan University, Japan. To obtain a well-defined regularly crystallized sample, ^{13}C antamanide was recrystallized from a mixture of methanol/water (7:3). The resulting needle-like crystals (50 mg) were ground into a

uniform powder prior to being inserted into the MAS rotor. It was found that the care in crystallization strongly influenced the attainable spectral resolution. Crystal defects, caused by improper crystallization, can lead to an undesired chemical shift inhomogeneity.

The NMR experiments for the ^{13}C assignment were performed on a Bruker DMX-400 NMR spectrometer equipped with a 4 mm Bruker triple-resonance MAS probe head. The spinning rate was controlled within ± 2 Hz by a Bruker MAS control unit.

Two-dimensional proton-driven spin-diffusion experiments were used for the intrasidue and sequential assignment and for the detection of long-range contacts. Standard Hartmann-Hahn cross-polarization proved to be efficient at a spinning rate of 15 kHz. During evolution and detection periods, heteronuclear TPPM decoupling (Bennett et al., 1995) was applied with a field strength of 71.4 kHz to efficiently remove the broadening by proton-carbon couplings. In key experiments, requiring optimum resolution, homonuclear ^{13}C decoupling by a pair of selective and non-selective π pulses (Straus et al., 1996) during the evolution period was used, as indicated in Fig. 1. This scheme allows complete homonuclear decoupling of a selected region in the ω_1 dimension of a 2D ^{13}C spectrum. The Gaussian pulse shape was generated with the program xShape, which is part of the Bruker XWIN-NMR package, using 256 points with a truncation value of 3%. The Gaussian pulse length was set to 800 μs for all experiments. Its amplitude was calibrated based on its inversion properties in the test experiment cross-polarization- $\pi/2$ (hard)- π (selective)- $\pi/2$ (hard), with simultaneous ^1H TPPM decoupling. The proton $\pi/2$ pulse length was 3.5 μs ($\omega_1/2\pi = 71.4$ kHz) and the carbon $\pi/2$ pulse length was 3.8 μs ($\omega_s/2\pi = 65.8$ kHz). The length and phase of the pulses for TPPM were optimized for maximum resolution. For a spinning speed of 15 kHz, it was found that the optimal pulse length is 6 μs and the optimal phases are $\pm 13^\circ$. The 2D experiments with homonuclear J decoupling were performed with a reduced sweep width of 10 kHz in ω_1 and $t_{1,\text{max}} = 22$ ms. All spectra were recorded at room temperature.

The ^{13}C T_1 relaxation experiments used recrystallized natural abundance antamanide to avoid undesired contributions from dipolar ^{13}C - ^{13}C relaxation. The experiments were performed on a Bruker MSL-400 NMR spectrometer. A 4 mm Doty MAS probe head was used for the measurements. The spinning rate was set to 6 kHz. The proton $\pi/2$ pulse was 3.1 μs ($\omega_1/2\pi = 80.6$ kHz) and the carbon $\pi/2$ pulse was 3.1 μs ($\omega_s/2\pi = 80.6$ kHz). After cross-polarization, the carbon magnetization was flipped along the $-z$ axis and then allowed to relax under CW proton decoupling. After this relaxation delay, a carbon $\pi/2$ pulse followed, and the ^{13}C spectrum was acquired under proton CW decoupling. A total of 1024 scans were taken and, prior to Fourier transformation, the FIDs

were apodized with a cosine-squared window. Six mixing times were taken (20 μ s, 10 ms, 100 ms, 500 ms, 5 s, 10 s). The line widths and peak positions of the longest mixing time were fitted using Lorentzian line shapes and these values were then used for fitting all the spectra adjusting the intensities only.

^{13}C Resonance assignment

For the assignment of fully isotope-labelled peptides or proteins in the solid state, dipolar correlation spectra (Meier, 1994) or possibly J-correlated spectra (Ramamoorthy et al., 1993; Baldus and Meier, 1996) can be used. For intrasidue assignment, the connectivity between the carbon atoms within one amino acid residue can be established using short mixing times, where predominantly nearest-neighbour transfers occur. Spectra recorded at longer mixing times provide interresidue information, allowing for a sequential assignment.

The resonance assignment is based on fully ^{13}C -labelled antamanide. The strategy followed here is analogous to that described by Balaban et al. (1995), with the difference that only ^{13}C labelling is used and that the resolution in the ω_1 dimension is enhanced by homonuclear decoupling (Straus et al., 1996). Proton-driven spin diffusion is used to correlate the ^{13}C spins.

The large quadrupolar moment of the ^{14}N spins is

known to lead to a ^{13}C line splitting of 35–44 Hz at 9.4 T, because of the residual dipolar interaction which is not averaged by MAS (Olivieri et al., 1987). This increases the line width of all the ^{13}C spins directly bound to ^{14}N . For assigning antamanide this does not pose significant problems, but for bigger proteins ^{15}N labelling and ^{15}N J decoupling is mandatory.

For the intrasidue assignment, spin-diffusion spectra with short mixing times (e.g. 12 ms) were used. In a second set of experiments, a slightly longer mixing time of 32 ms was selected, where already multiple-step nearest-neighbour transfers occur which are, however, restricted to intrasidue connectivities. Interresidue cross peaks have still very low intensities under these conditions. This allows one to trace out the intrasidue connectivities for the different amino acid residue types in analogy to the J-correlation procedures in the liquid phase (Wüthrich, 1986).

Figure 2a illustrates the intrasidue assignment for the two valine rotamer conformations Val_I^1 and Val_{II}^1 (see the section ‘Valine rotamer conformations’). The chemical shift frequencies of the methyl groups Val_I^1 $\text{C}_I^{\gamma 1}$ and Val_{II}^1 $\text{C}_{II}^{\gamma 1}$ along ω_1 are connected by cross peaks to all the other carbon resonances of Val along ω_2 : $\text{C}_I^{\gamma 2}$, C_I^β , C_I^α , C_I^δ , and similarly for the second conformer. The two families of cross peaks can uniquely be identified in this homonuclear ω_1 -decoupled spectrum. On the other hand, without

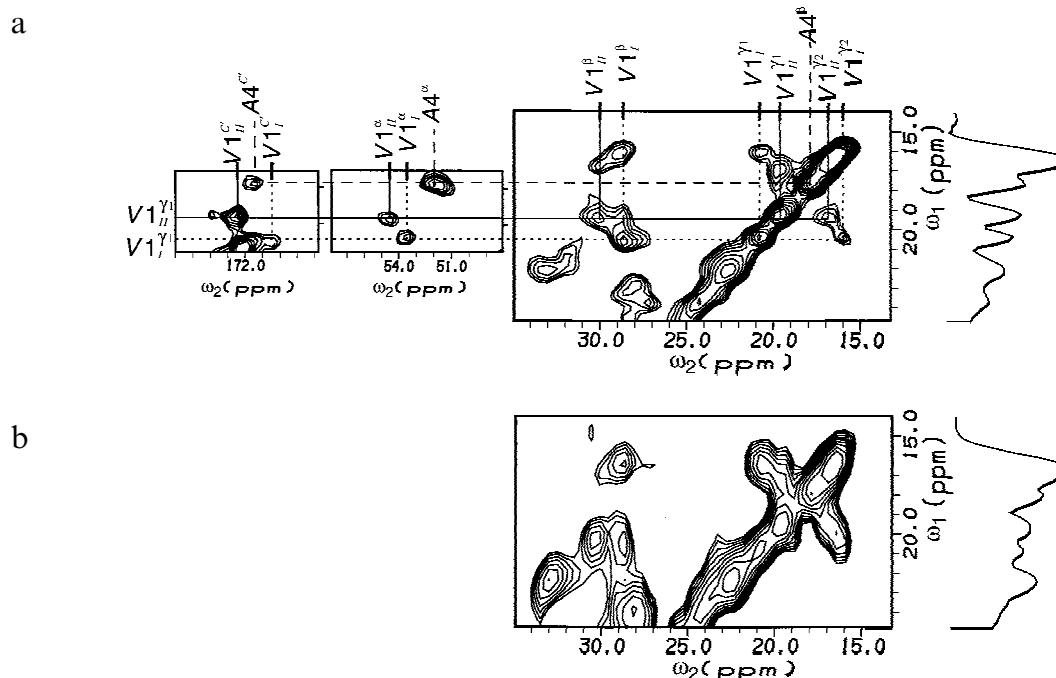


Fig. 2. Two-dimensional ^{13}C spectra of fully ^{13}C -labelled antamanide, recorded at 100 MHz carbon frequency and room temperature, displaying the connectivities for the two valine rotamers and for alanine: (a) with homonuclear decoupling in ω_1 ; (b) without homonuclear decoupling. The spectra were acquired with a mixing time of 32 ms and a spinning speed of 15 kHz. The 1D spectra on the right side of the 2D planes are the projections onto ω_1 . Both spectra, referenced with respect to TMS, are plotted at the same amplitude level, with the contour levels increasing by a factor of 1.2. In (a), 96 transients were added, resulting in a total experiment time of 20 h. In (b), 32 transients were added, resulting in a total experiment time of 14 h.

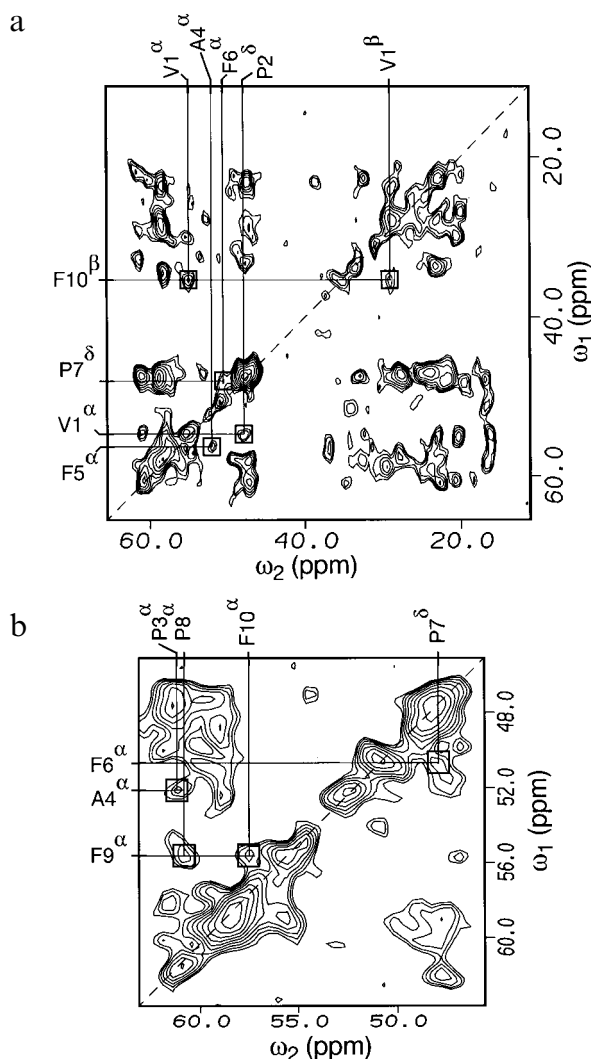


Fig. 3. Two-dimensional ^{13}C spectra of fully ^{13}C -labelled antamanide, with long mixing times for interresidue cross peaks (see text): (a) no homonuclear decoupling ($\tau_m = 150$ ms); (b) with homonuclear decoupling in ω_1 ($\tau_m = 100$ ms). The other parameters are the same as indicated in the caption of Fig. 2. Boxes indicate some of the cross peaks used to establish the sequential connectivities. Some of the cross peaks apparent in (a) are missing in (b). It was found that the observability of certain cross peaks strongly depends on the mixing time τ_m , which is different in (a) and (b).

is no longer possible due to severe overlap of the relevant cross peaks. The effect of ω_1 decoupling can also be appreciated from the projections onto the ω_1 axis, illustrated in Fig. 2. Connectivities for the other amino acids were also identified in a similar manner. Errors in the chemical shift values obtained were estimated by comparing the shifts in spectra recorded at different mixing times. The standard deviations amount to 0.2 ppm for well-separated peaks and can increase up to 0.6 ppm for strong overlap.

The sequential assignment of the residues was based on ^{13}C -coupled and ^{13}C - ω_1 -decoupled proton-driven spin-diffusion spectra with mixing times of 100 and 150 ms. An example of a ^{13}C -coupled spectrum is given in Fig. 3a,

while in Fig. 3b a blow-up of a ^{13}C - ω_1 -decoupled spectrum is shown. It is apparent that there is little symmetry with respect to the diagonal. This is attributed to differences in the cross-polarization rates and rotating frame relaxation times (Tuzi et al., 1992) for the different ^{13}C 's. This has been verified by varying the cross-polarization time. This deficiency, due to differences in the cross-polarization efficiency, could be alleviated by using improved cross-polarization procedures, such as AMCP (Hediger et al., 1995), where the transfer rate becomes more uniform. For assigning the four prolines, the known presence of two cis Xyz-Pro (Pro³ and Pro⁸) and two trans Xyz-Pro peptide bonds (Pro² and Pro⁷) was used (Karle et al., 1979). It is known that the conformation characteristically influences the proline chemical shift differences $\delta_{\text{C}^\beta} - \delta_{\text{C}^\gamma}$ with a range of 8–12 ppm for a cis peptide bond and 2–6 ppm for a trans peptide bond (Sarkar et al., 1984).

Based on the intrasidue assignment described above and the knowledge on the proline chemical shifts, interresidue connectivities were searched for. A set of interresidue cross peaks sufficient for completing the full sequential assignment is marked by boxes in Figs. 3a and b. For instance, one can identify a cross peak between C $^\alpha$ of Ala⁴ and C $^\alpha$ of Phe⁵, thus allowing one to distinguish this particular phenylalanine from the other three. Starting from Val¹ C $^\alpha$, one can identify a contact to Phe¹⁰ C $^\beta$. One can also see a cross peak between a Phe $^\alpha$ and a trans-bonded Pro ^{δ} resonance. Since this is only possible for Phe⁶ and Pro⁷, given the primary structure of antamanide, Phe⁶ and Pro⁷ can be assigned. By exclusion the other trans proline must be Pro² and the remaining phenylalanine connectivity pattern must be Phe⁹. The assignment of Pro² is additionally confirmed by a cross peak to Val¹ and that of Phe⁹ by a cross peak to Phe¹⁰ in the decoupled spectrum in Fig. 3b. One can also identify a contact between Phe⁹ and a proline C $^\alpha$, which again due to the primary structure must be Pro⁸. This allows one to distinguish Pro³ from Pro⁸.

The resulting solid-state assignment is summarized in Table 1. It is consistent with the liquid-state assignment of antamanide in chloroform (Bremi, 1993). The difference between the solid- and liquid-state chemical shifts, given in parentheses in Table 1, can be either due to environmental shifts or, more likely, are caused by the shift of conformational equilibrium due to the crystal packing.

Comparison of NMR data with X-ray structure

To compare the backbone structure determined by X-ray crystallography and that observed by solid-state NMR, the X-ray structure of antamanide was inspected for possible short distances between remote residues within the peptide backbone. The most relevant contacts for determining the conformation of the backbone are those across the peptide ring. In Fig. 4a, the shortest C $^\alpha$ C $^\alpha$ cross-annu-

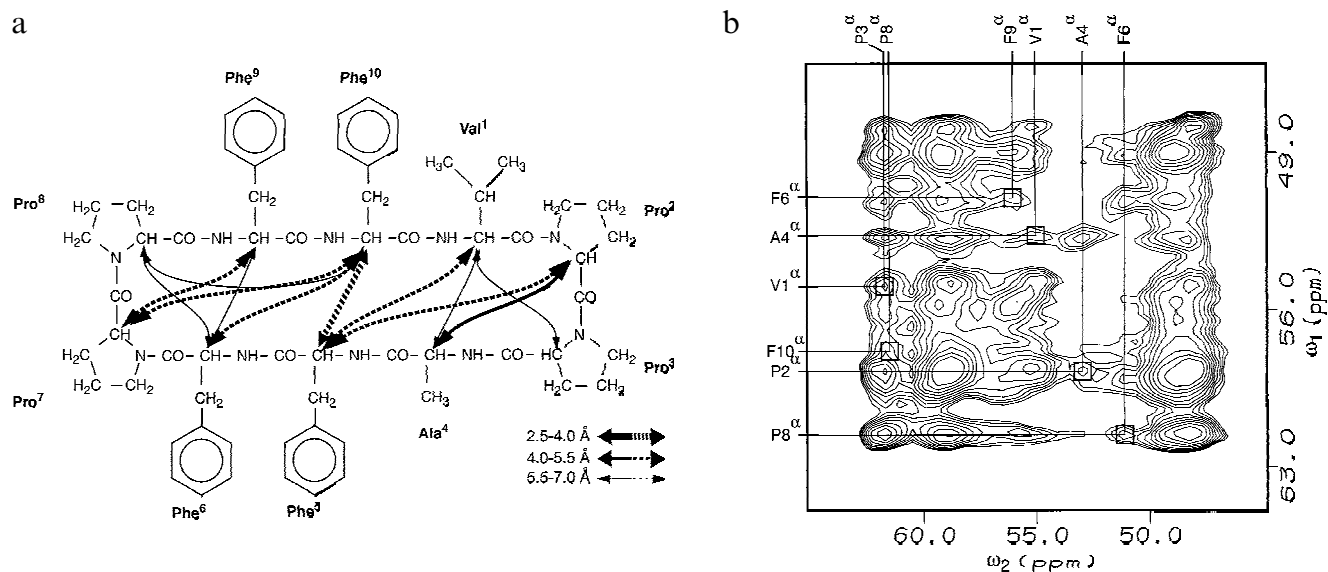


Fig. 4. Comparison of the NMR data with the X-ray structure. (a) Expected trans-annular $C^{\alpha}C^{\alpha}$ contacts based on the X-ray structure. Arrows drawn with solid lines represent contacts found in the NMR spectrum in (b). Those with broken lines indicate contacts whose cross peaks are likely to be hidden in the spin-diffusion spectrum. Three categories of distances are distinguished by the width of the arrows. In the range 5.5–7.0 Å, only those trans-annular contacts with clearly resolvable chemical shifts are indicated. (b) Two-dimensional proton-driven spin-diffusion spectrum with homonuclear decoupling in ω_1 and a mixing time of 250 ms. The other experimental parameters are the same as indicated in the caption of Fig. 2. The cross peaks due to trans-annular spin diffusion are indicated by boxes.

lar distances based on the X-ray crystal structure are indicated. Three classes of distances are encoded by the type of arrow used. A proton-driven spin-diffusion experiment allows only a qualitative estimate of the internuclear distance as the cross-relaxation rate constant depends also on the respective zero-quantum line shape function (Suter and Ernst, 1985). For more accurate distance determinations, it is advisable to use rf-driven pulse schemes where the ^{13}C - ^{13}C dipolar interactions are reintroduced in a controlled manner under MAS (Griffiths and Griffin, 1993; Meier, 1994).

As is apparent from Fig. 4b, long-range contacts expected from the X-ray structure appear in a spin-diffusion spectrum for an extended mixing time of 250 ms. For such a long mixing time, the spectrum becomes rather dense, resulting in overlapped cross peaks. For instance, the C^{α} - C^{α} cross peak of Phe⁵ and Phe¹⁰ situated near the diagonal cannot be resolved despite its expected large intensity based on Fig. 4a. This also renders a distinction between the cross peaks Val¹/Phe⁵ and Val¹/Phe¹⁰ impossible. Other long-range contacts, such as those between Pro²/Ala⁴, Phe⁶/Phe⁹, and Val¹/Ala⁴, are however visible.

TABLE 1
ASSIGNMENT OF ^{13}C RESONANCES IN ANTAMANIDE AT ROOM TEMPERATURE

Residue	CO (ppm)	C^{α} (ppm)	C^{β} (ppm)	C^{γ} (ppm)	C^{δ}
Val ¹ _I	171.0 ± 0.4 ^a (−0.2) ^b	53.5 ± 0.2 (3.1)	28.6 ± 0.2 (2.5)	20.5 ± 0.2 (−1.1)	–
Val ¹ _{II}	172.1 ± 0.4 (−1.3)	54.6 ± 0.2 (2.0)	30.0 ± 0.2 (1.1)	16.1 ± 0.2 (1.9)	–
Pro ²	171.3 ± 0.6 (−1.0)	59.2 ± 0.4 (−0.4)	29.1 ± 0.2 (−0.5)	24.7 ± 0.2 (0.5)	48.4 ± 0.4 (−0.5)
Pro ³	173.5 ± 0.2 (−2.7)	61.3 ± 0.2 (−0.2)	33.0 ± 0.2 (−1.4)	22.1 ± 0.6 (0.1)	48.7 ± 0.4 (−1.9)
Ala ⁴	171.7 ± 0.2 (2.3)	51.9 ± 0.2 (−2.0)	17.7 ± 0.2 (−0.5)	–	–
Phe ⁵	172.0 ± 0.6 (−1.2)	57.3 ± 0.4 (−0.3)	36.5 ± 0.2 (−0.6)	138.1 ± 0.6 (0.1)	131.6 ± 0.6 (−1.5)
Phe ⁶	172.5 ± 0.2 (0)	51.1 ± 0.2 (1.3)	37.3 ± 0.2 (−0.7)	138.0 ± 0.6 (−2.1)	^c
Pro ⁷	171.4 ± 0.6 (−1.1)	58.7 ± 0.4 (−0.2)	28.0 ± 0.2 (0.3)	23.6 ± 0.2 (1.4)	49.2 ± 0.4 (−1.6)
Pro ⁸	171.8 ± 0.2 (−2.1)	60.7 ± 0.2 (0.2)	32.4 ± 0.2 (−1.1)	21.8 ± 0.6 (−0.6)	47.5 ± 0.4 (−1.0)
Phe ⁹	174.5 ± 0.6 (−1.2)	55.7 ± 0.2 (1.6)	37.6 ± 0.2 (0.4)	139.6 ± 0.6 (−2.4)	^c
Phe ¹⁰	170.9 ± 0.6 (0.4)	57.7 ± 0.4 (1.2)	34.3 ± 0.2 (1.0)	139.1 ± 0.6 (−9.1)	131.5 ± 0.6 (−3.5)

Referenced to external adamantane ($\delta_{\text{CH}_2} = 38.56$ ppm and $\delta_{\text{CH}} = 29.50$ ppm with respect to TMS (Earl and VanderHart, 1979)).

^a See text.

^b Values in parentheses indicate the shift difference between the liquid state and the current assignment ($\delta_{(l)} - \delta_{(s)}$).

^c Not assigned.

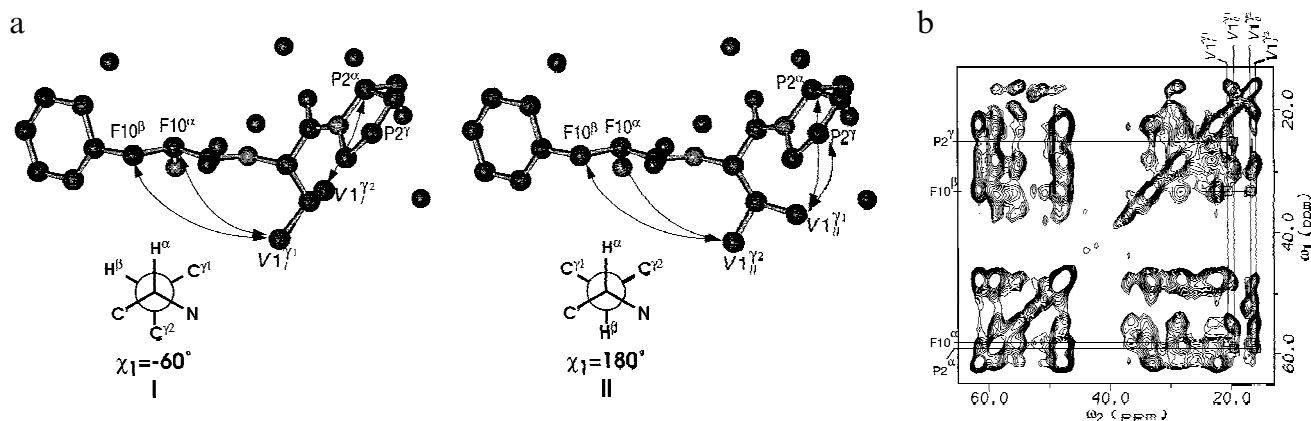


Fig. 5. Stereospecific assignment of the valine resonances. (a) Pictorial representation of the two valine rotamers with the two neighbouring residues Phe¹⁰ and Pro². The drawings are based on the X-ray structure. For conformer II, only the rotation angle χ_1 of Val¹ was changed. The contacts used for the stereospecific assignment are indicated with arrows. (b) Proton-driven spin-diffusion spectrum with a mixing time of 100 ms. The boxes indicate the cross peaks marked by arrows in (a). The other experimental parameters are the same as indicated in the caption for Fig. 2b.

The connections marked by solid arrows in Fig. 4a are indicated with boxes in the spectrum in Fig. 4b. Based on these contacts and others observed for different mixing times, it is concluded that the NMR data are not in contradiction with the structure determined by X-ray crystallography.

Valine rotamer conformations

As discussed in the section ¹³C resonance assignment, two sets of peaks can be identified for Val¹: one pair with C^γ chemical shift values of 16.1 and 20.5 ppm, and another pair with chemical shift values of 17.1 and 19.5 ppm. Several possibilities have to be considered for this doubling of peaks. One possibility is the presence of two crystal forms. Then one would expect a doubling of more peaks than just those of valine, in analogy to the situation in many crystalline amino acids, such as arginine hydrochloride (Straus et al., 1996). For antamanide, only the peaks of the valine residue are doubled (Table 1), rendering this hypothesis rather improbable.

A more likely explanation is the presence of two of the three possible χ_1 rotamers of Val¹, illustrated in Fig. 5a. For the first one with a torsion angle of $\chi_1 = -60^\circ$, which is found in the X-ray structure (Karle et al., 1979), the Val¹ C^{γ1} is relatively close to Phe¹⁰ C^α (distance: 4.7 Å) and Phe¹⁰ C^β (distance: 5.5 Å) and the Val¹ C^{γ2} is close to Pro² C^α (distance: 4.9 Å) and Phe¹⁰ C^α (distance: 5.2 Å). The distance to Pro² C^γ, on the other hand, is relatively large (distance >6.2 Å). For the second rotamer, with a torsion angle of $\chi_1 = 180^\circ$, Val¹ C^{γ1} is close to Pro² C^α (distance: 4.3 Å) and Pro² C^γ (distance: 4.1 Å). For Val¹ C^{γ2}, on the other hand, close contacts are found with Phe¹⁰ C^α (distance: 4.7 Å) and Phe¹⁰ C^β (distance: 5.5 Å). The third rotamer, with a torsion angle of $\chi_1 = +60^\circ$, entails two very strong contacts between Val¹ C^{γ1} and Pro² C^α (distance: 4.9 Å) and Phe¹⁰ C^α (distance: 5.2 Å).

Val¹ C^{γ2} for this third rotamer is close to Pro² C^α (distance: 4.3 Å) and Pro² C^γ (distance: 4.1 Å). A proton-driven spin-diffusion spectrum (Fig. 5b), with a mixing time of 100 ms, suggests that the first and the second rotamers are present. For the Val¹ C^γ pair at 16.1 and 20.5 ppm, we find cross peaks to Pro² C^α, Phe¹⁰ C^α and Phe¹⁰ C^β, but none to Pro² C^γ. This indicates that this pair of resonances corresponds to the rotamer with $\chi_1 = -60^\circ$ found in the crystal structure and that the stereospecific assignment of the ¹³C resonances is as follows: C^{γ2}_I, 16.1 ppm; C^{γ1}_I, 20.5 ppm. For the other Val¹ C^γ pair of resonances at 17.1 and 19.5 ppm, cross peaks are found between the resonance at 17.1 ppm and both Phe¹⁰ C^α and Phe¹⁰ C^β, and between the resonance at 19.5 ppm and Pro² C^α and Pro² C^γ, indicating that this is rotamer II with $\chi_1 = 180^\circ$. This also allows a stereospecific assignment of the resonances: C^{γ2}_{II}, 17.1 ppm; C^{γ1}_{II}, 19.5 ppm. The presence of cross peaks from Val¹ C^γ and Val¹ C^γ to Phe¹⁰ C^β excludes rotamer III with $\chi_1 = 60^\circ$. The conformational heterogeneity also induces slight chemical shift differences of the other valine resonances (see Table 1). It is therefore concluded that the two different sets of resonances indeed arise from two χ_1 rotamers. Exchange measurements performed on an unlabelled sample indicate that if there is exchange between the two rotamers in the solid state at all, the exchange-time constant must be significantly larger than 5 s.

It is revealing to compare the above findings with the corresponding rotamer analysis in liquid state. Based on three-bond J-coupling information, Schmidt (1997) could characterize the dynamic conformational equilibrium of the valine side chain of antamanide dissolved in chloroform by the presence of the three rotamers I ($\chi_1 = -60^\circ$), II ($\chi_1 = 180^\circ$) and III ($\chi_1 = 60^\circ$), with respective populations of 47%, 34% and 19%. In solution there is only one set of narrow resonances for the valine side chain, due to an interconversion which is significantly faster than the

difference between the chemical shifts of the conformers. Assuming that the chemical shift difference observed at 100 MHz in the solid state (~ 1 ppm = 100 Hz) is also valid in solution, the time constant of these interconversions has to be shorter than 2 ms. The two dominantly populated rotamers in liquid state are I and II, which is in agreement with the findings presented here. Also the stereospecific assignment in the solid state is consistent with that in CDCl_3 solution which is based on the $^3J(\text{H}^\alpha, \text{C}^{\gamma^i})$ coupling constants (Schmidt, 1997), assigning C^{γ^1} to the resonance at 19.4 ppm and C^{γ^2} to the resonance at 17.9 ppm. The possibility to investigate individual rotamers and to determine their chemical shifts therefore allows an estimation of an upper bound of the interconversion time constant in the liquid state.

The rotamer-dependent chemical shifts observed also for the other resonances of the valine residue imply that these ^{13}C resonances in the liquid phase would also be affected by a conformational exchange process of the side chain and not only by the dynamics of the backbone. An occasional broadening of $^{13}\text{C}^\alpha$ resonances does not necessarily indicate an exchange process involving the backbone, but can also be due to side-chain dynamics. It may even influence ^{15}N resonances.

Methyl-group rotation in solid antamanide

As pointed out by Batchelder et al. (1983), methyl-group rotation can be used as a sensitive probe for molecular packing effects because the rotational correlation times vary in a broad range, from a few picoseconds to several nanoseconds, due to interactions with the surroundings. Methyl-group relaxation in the solid state has been the issue of many investigations in the past (Andrew et al., 1976; Akasaka et al., 1983; Spiess, 1985; Beshah et al., 1987; Beshah and Griffin, 1989; Schleicher et al., 1990). Deuterium relaxation measurements on methyl-group rotation in amino acids proved to be especially informative, indicating a three-site jump process (Beshah et al., 1987). While at low temperatures tunnelling effects play a significant role, at room temperature the motional process can be described classically by a three-site jump process with a single correlation time (Press, 1981; Linder, 1982). Also in the liquid state, methyl-group ^{13}C relaxation in biopolymers has recently attracted attention (Nicholson et al., 1992; Palmer et al., 1993; Wand et al., 1996). There, the rotational jump process is partially masked by the overall tumbling, and the time constants in the range between 5 and 100 ps are rather ill-determined.

The χ_1 conformational static disorder found for Val¹ is due to steric interactions of the methyl groups with the environment. It is to be expected that these interactions also lead to effects on the methyl rotation. This motivated the study of methyl ^{13}C T_1 relaxation times presented in this section. The relaxation measurements are described

in the Experimental section. The unequal relaxation of the different methyl groups is apparent from Fig. 6, which shows spectra for four different relaxation recovery times. The resulting T_1 values are listed in Table 2.

The T_1 data were analysed using a three-site jump model for the intramolecular methyl-group motion. The general expression for the interpretation of longitudinal dipolar relaxation of a ^{13}C nucleus rigidly attached to N protons in the solid state is given by (Abragam, 1961)

$$\left(\frac{1}{T_1}\right) = N \frac{1}{20} \left(\frac{\mu_0}{4\pi}\right)^2 \left(\frac{h}{2\pi}\right)^2 \gamma_C^2 \gamma_H^2 \langle r_{\text{CH}}^{-3} \rangle^2 \times \{J_0(\omega_C - \omega_H) + 3J_1(\omega_C) + 6J_2(\omega_C + \omega_H)\} \quad (1)$$

where γ_C, γ_H and ω_C, ω_H are the gyromagnetic ratios and the Larmor frequencies of the carbon and the proton, respectively, and r_{CH} is the internuclear distance. Other relaxation mechanisms, like chemical-shielding-anisotropy and spin-rotation relaxation, can be neglected for methyl groups (Spiess et al., 1973; Spiess, 1978). The auto-spectral density functions $J_k(\omega)$, $k = -2, -1, 0, 1, 2$, are given as the Fourier transforms of the auto-correlation functions:

$$J_k(\omega) = \int_{-\infty}^{\infty} C_k(t) e^{-i\omega t} dt \quad (2)$$

with

$$C_k(t) = 4\pi \langle Y_{2k}(\Omega^{\text{lab}}(t)) Y_{2k}^*(\Omega^{\text{lab}}(0)) \rangle \quad (3)$$

and the normalized second-rank spherical harmonics $Y_{2k}(\Omega^{\text{lab}})$, where Ω^{lab} indicates the pair of polar angles of the considered C–H vector in the laboratory frame (Zare, 1988).

To express an intramolecular axial motion in the presence of magic angle spinning in the laboratory frame, the following two transformations are necessary:

(1) transformation from the coordinate system C of the crystal (chosen such that the z axis is along the axis of motion) to the spinner-fixed frame S with the Euler angles $\Phi_{\text{CS}} = (\alpha_{\text{CS}}, \beta_{\text{CS}}, \gamma_{\text{CS}})$; and

(2) transformation from the spinner-fixed frame S to the laboratory frame L with $\Phi_{\text{SL}} = (\alpha_{\text{SL}}, \beta_{\text{SL}}, \gamma_{\text{SL}})$.

For a sample spinning frequency ν_{MAS} much higher than the non-spinning relaxation rate constants, it is permitted to average over all values of the spinner phase α_{SL} using the relation $\langle e^{-i\alpha_{\text{SL}}} e^{i\alpha_{\text{SL}}} \rangle = \delta_{ll'}$. Choosing the laboratory frame such that γ_{SL} is zero and using the transformation properties of spherical harmonics (Zare, 1988), one gets the average correlation functions

$$\bar{C}_k(t) = 4\pi \sum_{l=-2}^2 [d_{lk}^{(2)}(\beta_{\text{SL}})]^2 \sum_{m, m'=-2}^2 d_{ml}^{(2)}(\beta_{\text{CS}}) d_{m'l}^{(2)}(\beta_{\text{CS}}) \times e^{-i\alpha_{\text{CS}}^{\text{qs}}(m-m')} C_{mm'}(t) Y_{2m}(\Omega^{\text{C}}) Y_{2m'}^*(\Omega^{\text{C}}) \quad (4)$$

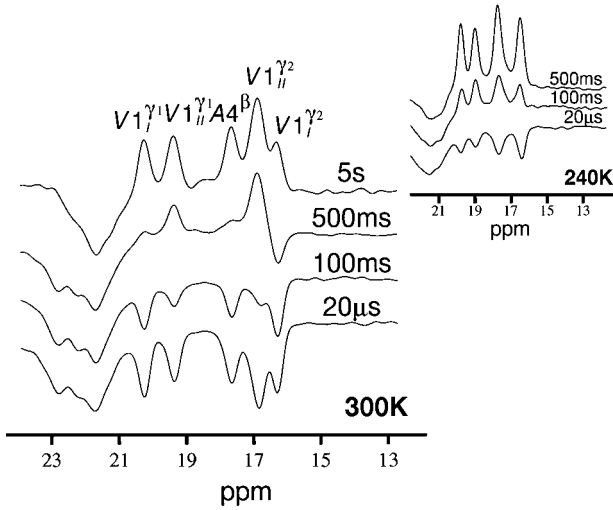


Fig. 6. T_1 relaxation of the methyl region of antamanide at 300 K and a magnetic field of 9.4 T. Four spectra are shown at the indicated delay after the initial π pulse. The inset shows the inversion-recovery behaviour of the same region at 240 K.

with

$$C_{mm}(t) = \langle e^{-im\alpha_{CM}(0) + im\alpha_{CM}(t)} \rangle \quad (5)$$

β_{SL} is the angle between the spinner axis and the static magnetic field, α_{CS}^{eq} describes one of the three equilibrium positions about the axis of rotation of the methyl group, and β_{CS} is the angle between the crystal-fixed frame z_C axis and the z_S axis of the coordinate system of the spinner. The crystal-fixed frame is chosen such that the z_C axis points along the rotation axis of the methyl group, namely the $C^\alpha C^\beta$ axis in the case of alanine and the $C^\beta C^{\gamma I}$ for valine. The polar angles Ω^C give the orientation of the dipolar interaction in the crystal system.

Even if β_{SL} is at the magic angle, Eq. 4 still contains an orientational dependence ($\alpha_{CS}^{eq}, \beta_{CS}$) unless $C_{mm}(t) = \delta_{m,m} C_{mm}(t)$. The latter condition is fulfilled for certain motional models. The orientational dependence leads to an observed signal consisting of a superposition of spectral lines having different relaxation properties.

For a symmetric three-site jump model with equal populations, $C_{m,m}(t)$ can be evaluated by standard methods (Brüschweiler and Case, 1994), leading to

$$C_{mm}(t) = \delta_{m,0}\delta_{m',0} + (\delta_{m,m'} + \delta_{m,-m'/2} + \delta_{m/2,-m'} - 3\delta_{m,0}\delta_{m',0})e^{-t/\tau} \quad (6)$$

where $\tau^{-1} = 3k$ with the jump rate constant k . Clearly, the matrix $C_{mm}(t)$ is not diagonal and the resulting relaxation behaviour is non-exponential. However, restricting the relaxation measurement to the linear initial regime, the relevant correlation functions can be evaluated by averaging over all values of β_{CS} , leading to (Torchia and Szabo, 1982)

$$\bar{C}_k(t) = 4\pi \sum_{m=-2}^2 \langle e^{-im\alpha_{CS}(0) + im\alpha_{CS}(t)} \rangle Y_{2m}(\Omega^C) Y_{2m}^*(\Omega^C) \quad (7)$$

For the evaluation of $1/T_1$ according to Eq. 1, ideal tetrahedral geometry and a CH bond length of 1.09 Å were assumed (Ernst and Ernst, 1994). Since the data were taken at one magnetic field only, two solutions exist for the correlation time of the jump process and a further measurement is necessary to check whether the motion is in the fast or in the slow motion regime. The relaxation proceeds faster at 240 K (see the inset in Fig. 6) than at room temperature. Moreover, the relaxation behaviour of the methyl groups is more uniform at the lower temperature. This leads to the conclusion that at room temperature the motion is in the fast motional regime, and that at 240 K the relaxation is, for all the methyl groups, close to the T_1 minimum, where the motional dependence of T_1 becomes small. The determined correlation times of the jump processes of the five methyl groups are listed in Table 2.

The jump correlation times are in the range of 5–100 ps, indicating little hindrance of the methyl-group rotation. The correlation time of the alanine methyl group in antamanide of 31.6 ps, compared with that observed in polycrystalline D-alanine of 1.6 ns (Andrew et al., 1976; Akasaka et al., 1983), is in agreement with the well-known loose packing of peptide crystals containing several water molecules. Additionally, the valine relaxation data agree with the low-temperature deuterium study on *N*-acetyl-DL-valine (Beshah and Griffin, 1989), where it is found that the two methyl groups have T_1 values that differ by an order of magnitude (extrapolating to room temperature, jump correlation times of approximately 200 and 40 ps are determined for the two methyl groups). In confor-

TABLE 2
 ^{13}C METHYL-GROUP RELAXATION DATA OF ANTAMANIDE IN THE SOLID STATE AT 300 K AND 400 MHz PROTON RESONANCE FREQUENCY^a

Parameter	Val ^I C _I ^{γ1} (20.5 ppm)	Val ^I C _{II} ^{γ1} (19.5 ppm)	Ala ⁴ C ^β (17.7 ppm)	Val ^I C _{II} ^{γ2} (17.1 ppm)	Val ^I C _I ^{γ2} (16.1 ppm)
T_1 (s) ^b	0.57 ± 0.08	0.29 ± 0.02	0.56 ± 0.02	0.21 ± 0.02	2.59 ± 0.36
τ_{jump} (ps) ^c	31.2 ± 4.3	61.3 ± 5.9	31.6 ± 2.1	89.0 ± 17.1	6.7 ± 1.2

^a The valine rotamers are labelled according to the conventions used in the text (I: $\chi_1 = -60^\circ$; II: $\chi_1 = 180^\circ$).

^b Standard deviations were estimated using error propagation.

^c τ_{jump} is defined as $(\tau_{\text{jump}})^{-1} = 3k$, where k is the jump rate constant between the sites.

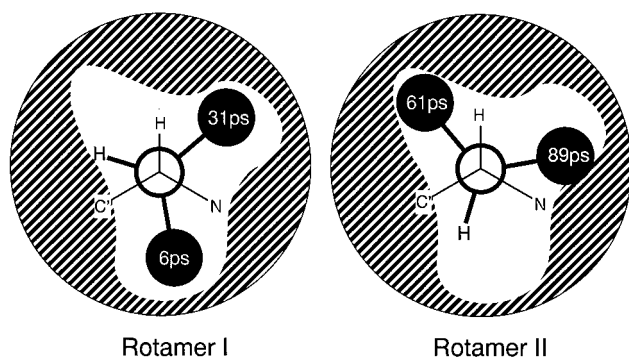


Fig. 7. Pictorial representation of the proposed model rationalizing the relaxation data of the two valine rotamers in antamanide in the solid state. The methyl groups are indicated as circles, and their rotational correlation times are also given. The hindering potential is indicated by hatched areas (see text).

mation II of valine in antamanide, the two methyl groups Val^I C_{II}^{γ1} and Val^I C_{II}^{γ2} rotate with similar jump time constants of 61.3 and 89.0 ps, respectively; the other conformer shows a more individual behaviour with 31.2 ps for Val^I C_I^{γ1} and 6.7 ps for Val^I C_I^{γ2}. It is interesting to note that although Val^I C_I^{γ1} and Val^I C_{II}^{γ2} occupy the same position in space (see Fig. 5a), their motional behaviour is different by a factor of 2.9. The small jump rate constant of Val^I C_I^{γ2}, contrasting with the values of all the other methyl groups, indicates that this resonance must be in a unique surrounding. An inspection of the crystal structure shows that, indeed, Val^I C_I^{γ2} sticks into the interior of the antamanide ring while the other three methyl groups stick towards the outside.

A possible model which rationalizes the experimental data is given in Fig. 7. The fact that rotamer III is not found can be explained by a strong steric hindrance in a large angular range (in the shaded area near C^γ; Fig. 7) allowing only the proton to be close to that region. The three regions of lower steric hindrance are asymmetric and not exactly differing by 120° in their χ_1 angles. In rotamer I the methyl group C^{γ2} is situated in a relatively wide potential energy minimum with little hindrance (see the above paragraph), leading to $\tau_{\text{jump}} = 6$ ps, being fixed there by the more restrained methyl group C^{γ1} with $\tau_{\text{jump}} = 31$ ps. The restraints for rotamer II are more pronounced, leading to longer values of τ_{jump} of 61 and 89 ps. It is impossible at this point to further specify the nature of the restraining interactions. It is well conceivable that, among others, also the interactions with the water molecules could be relevant.

Conclusions

In this paper we have shown that, with the resolution presently achievable by using optimized heteronuclear decoupling and homonuclear J decoupling, it is possible to derive detailed structural and dynamical information

from solid-state MAS spectra of fully ¹³C-labelled biomolecules. Assignment of the ¹³C resonances is possible without taking recourse to liquid-state information. Based on spin-diffusion experiments, it is also possible to stereospecifically assign side-chain resonances. While for the system studied here 2D spectra proved to be adequate, for larger peptides and proteins the assignment of ¹³C resonances will have to be based on 3D spectra with homonuclear decoupling in both indirect time dimensions (Straus et al., 1996). For fully ¹³C/¹⁵N-labelled systems, a set of triple-resonance experiments will be advantageous, correlating ¹³C and ¹⁵N nuclei along the backbone and side chains, as proposed, for example, by Tycko (1996).

Two rotamers of the valine side chain of antamanide coexisting in the solid state have been identified. They are found to agree with the predominant rotamers in the liquid state that were identified based on J-coupling information. Thus, the dynamical conformational equilibrium present in the liquid state is converted into conformational static disorder in the solid. Based on the chemical shift difference in the solid state, an upper bound for the rotational correlation time of 2 ms for the χ_1 rotation in the liquid phase at room temperature can be obtained. Furthermore, the methyl-group rotation for these two rotamers was found to depend in a characteristic manner on the rotamer orientation due to specific interactions with the surroundings.

Acknowledgements

We would like to thank Prof. S. Aimoto of the Institute of Protein Research, Osaka University, and Prof. M. Kainosho of the Department of Chemistry, Tokyo Metropolitan University, for supplying fully ¹³C-labelled antamanide. Stimulating discussions with PD Dr. R. Meyer, Christoph Scheurer and Dr. Bernhard Brutscher are gratefully acknowledged. S.K.S. would like to thank NSERC for their financial support. This work has been supported by the Swiss National Science Foundation.

References

- Abragam, A. (1961) *Principles of Nuclear Magnetism*, Oxford University Press, Oxford, U.K.
- Akasaka, K., Ganapathy, S., McDowell, C.A. and Naito, A. (1983) *J. Chem. Phys.*, **78**, 3567–3572.
- Andrew, E.R., Hinshaw, W.S., Hutchins, M.G., Sjöblom, R.O.I. and Canepa, P.C. (1976) *Mol. Phys.*, **32**, 795–806.
- Balaban, T.S., Boender, G.J., Holzwarth, A.R., Schaffner, K. and De Groot, H.J.M. (1995) *Biochemistry*, **34**, 15259–15266.
- Baldus, M. and Meier, B.H. (1996) *J. Magn. Reson.*, **A121**, 65–69.
- Batchelder, L.S., Niu, C.H. and Torchia, D.A. (1983) *J. Am. Chem. Soc.*, **105**, 2228–2231.
- Bennett, A.E., Rienstra, C.M., Auger, M., Lakshmi, K.V. and Griffin, R.G. (1995) *J. Chem. Phys.*, **103**, 6951–6958.
- Beshah, K., Olejniczak, E.T. and Griffin, R.G. (1987) *J. Chem. Phys.*, **86**, 4730–4736.

- Beshah, K. and Griffin, R.G. (1989) *J. Magn. Reson.*, **84**, 268–274.
- Blackledge, M.J., Brüschweiler, R., Griesinger, C., Schmidt, J.M., Xu, P. and Ernst, R.R. (1993) *Biochemistry*, **32**, 10960–10974.
- Bremi, T. (1993) Diplomarbeit, ETH Zürich, Zürich, Switzerland.
- Bremi, T., Ernst, M. and Ernst, R.R. (1994) *J. Phys. Chem.*, **98**, 9322–9334.
- Brüschweiler, R., Blackledge, M. and Ernst, R.R. (1991) *J. Biomol. NMR*, **1**, 3–11.
- Brüschweiler, R., Roux, B., Blackledge, M.J., Griesinger, C., Karplus, M. and Ernst, R.R. (1992) *J. Am. Chem. Soc.*, **114**, 2289–2302.
- Brüschweiler, R. and Case, D. (1994) *Prog. NMR Spectrosc.*, **26**, 27–58.
- Burgermeister, W., Wieland, T. and Winkler, R. (1974) *Eur. J. Biochem.*, **44**, 311–316.
- Earl, W.L. and VanderHart, D.L. (1979) *J. Magn. Reson.*, **48**, 35–54.
- Ernst, M. and Ernst, R.R. (1994) *J. Magn. Reson.*, **A110**, 202–213.
- Ernst, R.R., Blackledge, M.J., Bremi, T., Brüschweiler, R., Ernst, M., Griesinger, C., Mádí, Z.L., Peng, J.W., Schmidt, J.M. and Xu, P. (1996) In *NMR as a Structural Tool for Macromolecules: Current Status and Future Directions* (Eds. Rao, N. and Kempfle, M.D.), Plenum Press, New York, NY, U.S.A., pp. 15–30.
- Frey, M.H., Opella, S.J., Rockwell, A.J. and Gierasch, L.M. (1985) *J. Am. Chem. Soc.*, **107**, 1946–1951.
- Griffiths, J.M. and Griffin, R.G. (1993) *Anal. Chim. Acta*, **283**, 1081–1101.
- Griffiths, J.M., Ashburn, T.T., Auger, M., Costa, P.R., Griffin, R.G. and Lansbury Jr., P.T. (1995) *J. Am. Chem. Soc.*, **117**, 3539–3546.
- Hediger, S., Meier, B.H. and Ernst, R.R. (1995) *J. Chem. Phys.*, **102**, 4000–4011.
- Heller, J., Kolbert, A.C., Larsen, R., Ernst, M., Bekker, T., Baldwin, M., Prusiner, S.B., Pines, A. and Wemmer, D.E. (1996) *Protein Sci.*, **5**, 1655–1661.
- Hirsh, D.J., Hammer, J., Maloy, W.L., Blazyk, J. and Schaefer, J. (1996) *Biochemistry*, **35**, 12733–12741.
- Karle, I.L., Wieland, T., Schermer, D. and Ottenheim, H.C.J. (1979) *Proc. Natl. Acad. Sci. USA*, **76**, 1532–1536.
- Kessler, H., Griesinger, C., Lutz, J., Müller, A., van Gunsteren, W.F. and Berendsen, H.C.J. (1988) *J. Am. Chem. Soc.*, **110**, 3394–3396.
- Kessler, H., Bats, J.W., Lutz, J. and Müller, A. (1989a) *Liebigs Ann. Chem.*, **1989**, 913–928.
- Kessler, H., Müller, A. and Pook, K.-H. (1989b) *Liebigs Ann. Chem.*, **1989**, 903–912.
- Kessler, H., Griesinger, C. and Wagner, K. (1987) *J. Am. Chem. Soc.*, **109**, 6927–6933.
- Lansbury Jr., P.T., Costa, P.R., Griffiths, J.M., Simon, E.J., Auger, M., Halverson, K.J., Kociska, D.A., Hendsch, Z.S., Ashburn, T.T., Spencer, R.G.S., Tidor, B. and Griffin, R.G. (1995) *Nat. Struct. Biol.*, **2**, 990–998.
- Lazo, N.D. and Cross, T.A. (1995) *J. Magn. Reson.*, **B107**, 43–50.
- Linder, M. (1982) Ph.D. Dissertation (no. 7028), ETH Zürich, Zürich, Switzerland.
- Mádí, Z.L., Griesinger, C. and Ernst, R.R. (1990) *J. Am. Chem. Soc.*, **112**, 2908–2914.
- Meier, B.H. (1994) *Adv. Magn. Reson. Opt. Reson.*, **18**, 1–116.
- Müller, A. (1986) Ph.D. Dissertation, University of Frankfurt, Frankfurt, Germany.
- Naito, A., Nishimura, K., Tuzi, S. and Saito, H. (1995) *Pept. Chem.*, **1994**, 77–80.
- Nicholson, L.K., Kay, L.E., Baldissari, D.M., Arango, J., Young, P.E., Bax, A. and Torchia, D.A. (1992) *Biochemistry*, **31**, 5253–5263.
- Olivieri, A.C., Frydman, L. and Diaz, L.E. (1987) *J. Magn. Reson.*, **75**, 50–62.
- Opella, S.J., Stewart, P.L. and Valentine, K.G. (1987) *Q. Rev. Biophys.*, **19**, 7–49.
- Palmer III, A.G., Hochstrasser, R.A., Millar, D.P., Rance, M. and Wright, P.E. (1993) *J. Am. Chem. Soc.*, **115**, 6333–6345.
- Press, W. (1981) *Single Particle Rotations in Molecular Crystals*, Springer, Berlin, Germany.
- Ramamoorthy, A., Fujiwara, T. and Nagayama, K. (1993) *J. Magn. Reson.*, **A104**, 366–368.
- Sarkar, S.K., Torchia, D.A., Kopple, K.D. and VanderHart, D.L. (1984) *J. Am. Chem. Soc.*, **106**, 3328–3331.
- Schleicher, A., Müller, K. and Kothe, G. (1990) *J. Chem. Phys.*, **92**, 6432–6440.
- Schmidt, J.M., Brüschweiler, R., Ernst, R.R., Dunbrack Jr., R.L., Joseph, D. and Karplus, M. (1993) *J. Am. Chem. Soc.*, **115**, 8747–8756.
- Schmidt, J.M. (1997) *J. Magn. Reson.*, **124**, 298–309.
- Schmidt, J.M. (1997) *Supramol. Struct. Funct.*, to appear.
- Spiess, H.W., Schweitzer, D. and Haebleren, U. (1973) *J. Magn. Reson.*, **9**, 444–460.
- Spiess, H.W. (1978) *NMR Basic Principles Prog.*, **15**, 55–214.
- Spiess, H.W. (1985) *Adv. Polym. Sci.*, **66**, 23–58.
- Stewart, P.L., Tycko, R. and Opella, S.J. (1988) *J. Chem. Soc., Faraday Trans.*, **84**, 3803–3819.
- Straus, S.K., Bremi, T. and Ernst, R.R. (1996) *Chem. Phys. Lett.*, **262**, 709–715.
- Suter, D. and Ernst, R.R. (1985) *Phys. Rev.*, **B32**, 5608–5627.
- Torchia, D.A. and Szabo, A. (1982) *J. Magn. Reson.*, **49**, 107–121.
- Tuzi, S., Shinzawa-Itoh, K., Erata, T., Naito, A., Yoshikawa, S. and Saito, H. (1992) *Eur. J. Biochem.*, **208**, 713–720.
- Tycko, R. (1996) *J. Biomol. NMR*, **8**, 239–251.
- Wand, A.J., Urbauer, J.L., McEvoy, R.P. and Bieber, R.J. (1996) *Biochemistry*, **35**, 6116–6125.
- Wüthrich, K. (1986) *NMR of Proteins and Nucleic Acids*, Wiley, New York, NY, U.S.A.
- Zare, R. (1988) *Angular Momentum*, Wiley/Interscience, New York, NY, U.S.A.